Materials Science & Engineering C 96 (2019) 337–346

Contents lists available at ScienceDirect

Materials Science & Engineering C

journal homepage: www.elsevier.com/locate/msec

Ramification of zinc oxide doped hydroxyapatite biocomposites for the mineralization of osteoblasts

Puvala Vijayakumar Gnaneshwar[a,b,c], Shruthi Vathaluru Sudakaran[a], Sivasubramanian Abisegapriyan[a], Jositta Sherine[b], Seeram Ramakrishna[a], Mohd Hasbi Ab. Rahim[d], Mashitah Mohd. Yusoff[d], Rajan Jose[d], Jayarama Reddy Venugopal[a,d,*]

[a] Centre for Nanofibers & Nanotechnology, Mechanical Engineering, Faculty of Engineering, National University of Singapore, Singapore
[b] Department of Physics and Nanotechnology, SRM University, Kattankulathur, Chennai, India
[c] Nano Science and Technology Program, Taiwan International Graduate Program, Academia Sinica and National Tsing Hua University, Taiwan
[d] Faculty of Industrial Sciences & Technology, Universiti Malaysia Pahang, 26300, Gambang, Kuantan, Pahang, Malaysia

ARTICLE INFO

Keywords:
Bone tissue regeneration
Zinc oxide
Hydroxyapatite
Biocomposite
Osteoblasts
Mineralization

ABSTRACT

Far-flung evolution in tissue engineering enabled the development of bioactive and biodegradable materials to generate biocomposite nanofibrous scaffolds for bone repair and replacement therapies. Polymeric bioactive nanofibers are to biomimic the native extracellular matrix (ECM), delivering tremendous regenerative potentials for drug delivery and tissue engineering applications. It's been known from few decades that Zinc oxide (ZnO) nanoparticles are enhancing bone growth and providing proliferation of osteoblasts when incorporated with hydroxyapatite (HAp). We attempted to investigate the interaction between the human foetal osteoblasts (hFOB) with ZnO doped HAp incorporated biocomposite poly(L-lactic acid)-*co*-poly(ε-caprolactone) and silk fibroin (PLACL/SF) nanofibrous scaffolds for osteoblasts mineralization in bone tissue regeneration. The present study, we doped ZnO with HAp (ZnO(HAp) using the sol-gel ethanol condensation technique. The properties of PLACL/SF/ZnO(HAp) biocomposite nanofibrous scaffolds enhanced with doped and blended ZnO/HAp were characterized using Scanning electron microscopy (SEM), Fourier transform infrared spectroscopy (FTIR), Contact angle and Tensile studies to determine the morphology, functionality, wettability and stability. The *in vitro* study results showed that the addition of ZnO and HAp enhances the secretion of bone mineral matrix (98%) with smaller fiber diameter (139.4 ± 27 nm) due to the presence of silk fibroin showing potential tensile properties (322.4%), and increased the proliferation of osteoblasts for bone tissue regeneration.

1. Introduction

Strategy to repair and regenerate bones using the best combination of biomaterials with biodegradable polymers in bone tissue engineering. Maintain the existing bone tissue structure or to enable bone tissue growth, bone tissue engineering is one such aspect that utilizes both engineering and life science disciplines. Orthopaedic implants such as titanium and its alloys have an average functional regenerative lifespan of 10–15 years. Surface modification for metal implants are required to support the bone growth [1]. Detrimental wear debris as well as stress and strain imbalance at the tissue-implant interface, leading to loosening of the implant and inevitable failure due to poor integration of orthopaedic implants [2]. Recently, bone tissue engineering focused on the development of 3D scaffolds, which requires higher stability and biocompatibility. These scaffolds should fulfil the requirements such as interconnected microporous structure to support the cells and exchange of nutrients. The absorption kinetics, mechanical strength and adequate surface area of the scaffolds are also important for cell viability and scaffold durability [3,4]. Generally used polymers for tissue engineering applications such as polycaprolactone (PCL) [5], poly(lactide) [6], poly(glycolide) [6,7], poly(lactide-co-glycolide) [8], poly-L-lactic acid (PLLA) [9], polyorthoesters [10], poly(L-lactic acid)-*co*-poly(ε-caprolactone) (PLACL) [11], polyphospoesters, polyanhydrides, polyphosphazanes and polyethylene oxide.

PLACL is an elastomeric copolymer of PCL and PLLA was found to be potential synthetic biopolymer to fabricate nanofibers for bone tissue regeneration therapy [11] satisfies the material properties like high surface to volume ratio, osteoconductive, osteoinductive, non-

* Corresponding author at: Faculty of Industrial Sciences & Technology, Universiti Malaysia Pahang, Lebuhraya Tun Razak, 26300, Gambang, Kuantan, Pahang, Malaysia.
E-mail address: venugopal@ump.edu.my (J.R. Venugopal).

https://doi.org/10.1016/j.msec.2018.11.033
Received 16 January 2018; Received in revised form 16 August 2018; Accepted 23 November 2018
Available online 24 November 2018
0928-4931/

cytotoxicity, interconnectivity of pores for neovascularization at the site of new tissue regeneration, sufficient porosity for the transport of nutrients and regulatory factors [12]. Silk fibroin (SF), is a provisional matrix due to its importance in the early stages of wound healing, bone repair and for their excellent bioactive properties. SF is functional biomaterial with high elasticity, significant crystallinity, strength, resistance and toughness. Apart from being one of the important natural polymers for the better tensile strength of SF shows additional effects like good water vapour and oxygen permeability, slow degradation rate, minimal inflammatory response and ability to use in several forms with high endurance [13]. The nanoparticle allows their internalization into cells in greater extent and allows them to interact with biomolecules within or on the cell surface, enabling them to potentially affect cellular function in a dynamic and selective manner. There are many different metal and metal oxide nanoparticles like MgO [14,15], Ag [16], Fe_2O_3 [17], TiO_2 [18], CuO [19], $Mg(OH)_2$ [20] and ZnO [21,22] are used for various biomedical and biotechnology applications. Among which, zinc oxide nanoparticles (NPs) stand aside by showing its maximum antibacterial activity and excellent biocompatibility [21,22]. Recent studies have indicated that ZnO nanoparticles affected functions of different cells or tissues, biocompatibility and neural tissue engineering [23–25]. ZnO particles are currently listed as a 'Generally Recognized as Safe (GRAS)' material by the Food and Drug Administration and also used as a food additive and in many products.

Hydroxyapatite is highly biocompatible, biodegradable and has a greater identity with the inorganic component of vertebrate bone [26]. Recently, HAp has been used for numerous biomedical applications, including matrices for controlled drug delivery in bone tissue engineering [27]. HAp is generally doped with different trace elements to increase it's biological activity. Zinc being highly used metal oxide in medicines and having an important trace element in biological tissues, shows the activity of > 300 types of enzymes [28] are suitable for bone tissue engineering. Zinc-doped hydroxyapatite nanoparticles (ZnO/HAp) are biocompatible, have increased bioactivity, nucleic acid metabolism, enzyme activity and biomineralization [29]. Several studies have reported that the amount of zinc incorporates with HAp tend to show greater bone healing properties [30] despite the incorporation of zinc into HAp is based on the method and condition used for synthesis [31–33]. Recently, researchers found zinc ions are essential for various metabolic activities in most of the living organisms also shows the stimulatory effect on bone formation *in vitro* and *in vivo* [34]. The objective of this research is to synthesise ZnO nanoparticle doped with HAp along with PLACL/silk fibroin in a controlled environment and discussed the interaction with osteoblasts and its ability to enhance the secretion of ECM for mineralization in bone tissue regeneration.

2. Materials and methods

Human foetal osteoblast cells (hFOB) were obtained from American Type Culture Collection (ATCC, Arlington, VA). Antibiotics, foetal bovine serum (FBS), Dulbecco's Modified Eagle's Medium/Nutrient Mixture F-12 (HAM), trypsin-EDTA, polyvinylpyrrolidone (PVP), zinc acetate, absolute ethanol, 1,1,1,3,3,3-hexafluoro-2-propanol (HFP) and hexamethyl-disilazane (HMDS) were purchased from Sigma, Singapore. Poly(ι-lactic acid)-*co*-poly-ε-caprolactone (Mw 150 kDa) (70:30) was obtained from Boehringer Ingelheim Pharma, GmbH & Co., Ingelheim, Germany. CellTiter 96 AQueous One solution was purchased from Promega, Madison, WI, USA. Crystalline hydroxyapatite (Microwave method) and zinc oxide nanoparticles were synthesised in NUS-CNN, Singapore.

2.1. Synthesis of nanoparticles

2.1.1. Synthesis of zinc oxide nanoparticles

Zinc oxide nanoparticles were synthesised using ethanol condensation sol-gel process. To prepare ZnO nanoparticles, zinc acetate (5 mM) dissolved in 90 ml absolute ethanol for 15–20 min under low temperature (30 °C) in glycerol bath to provide localized uniform heating. Meanwhile, dissolve 0.90 g of PVP (Mw 150 kDa) in 10 ml of deionized water. After PVP dissolved completely then add the solution to zinc acetate ethanol mixture drop-wise and continue stirring for 1 h. After 1 h stirring use water condensation and stir overnight. Collect the sample and heat treat at 100 °C for 2 h followed by calcination at 300 °C.

2.1.2. Synthesis of zinc oxide doped hydroxyapatite

Synthesis of zinc oxide doped hydroxyapatite (ZnO/HAp), 5 mM zinc acetate was dissolved in 90 ml absolute ethanol for 15 min under continuous stirring. Add 0.45 g HAp and continue stirring for another 30 min. Dissolve 0.90 g of PVP in 20 ml of deionized water. Add PVP solution dropwise into the precursor solution and stir with minimum rpm at 90 °C for 24 h under ethanol condensation system. After 24 h collected the samples and dry at 50 °C for 2 h then anneal at 120 °C for 8 h.

2.2. Fabrication of nanofibrous scaffolds

Electrospinning of prescribed nanofibers requires the optimisation of various parameters including voltage, flow rate, distance between the tip and substrate, viscosity of the solution, homogeneity of the solution. PLACL was dissolved in HFP to obtain 15% wt. solution and electrospun at a voltage of 13.5 kV at a stipulated distance of 10–13 cm. PLACL and synthesised zinc oxide nanoparticles mixed in HFP solvent with a weight percent of 14% and 1% respectively. Similarly, PLACL, silk fibroin and zinc oxide particles were dissolved in HFP at 13:1:2, all these solvents are kept stirring overnight to form a uniform homogeneous solution without lumps and air bubbles. The samples PLACL/SF/ZnO/HAp and PLACL/SF/ZnO(HAp) are prepared in the ratio of 12:1:1:1 and 12:1:2 respectively and left stirring overnight. The final concentration of all the polymer blends kept constant at 15%. The details of electrospun fibers and their solution parameters are given in Table 1. The fabricated nanofibers are kept at an ambient temperature of 22–25 °C and relative humidity of 40–60%.

2.3. Characterization of nanofibrous scaffolds

Morphological studies of PLACL, PLACL/ZnO, PLACL/SF/ZnO, PLACL/SF/ZnO/HAp and PLACL/SF/ZnO(HAp) electrospun biocomposite nanofibers were analysed using Field Emission Scanning Electron Microscope (JEOL JSM 6700, Japan) at an acceleration voltage of 10 kV, after sputter coating with gold (JEOL JFC-1200 Fine Coater, Japan). Structural analyses performed with SEM images, using image

Table 1
Electrospinning parameters for the fabrication of nanofibers.

S/No	Samples	Concentration (%)	Voltage (kV)	Flow rate (ml/h)	Needle size	Fiber diameter (nm)
1	PLACL	15	13.5	1.5	22G	627.3 ± 103
2	PLACL/ZnO	14:1	13	1	22G	715.4 ± 190
4	PLACL/SF/ZnO	13:1:2	13.5	1	23G	192 ± 69
5	PLACL/SF/ZnO/HAp	12:1:1:1	15	1	23G	156.6 ± 53
6	PLACL/SF/ZnO(HAp)	12:1:2	15	1	23G	139.4 ± 27

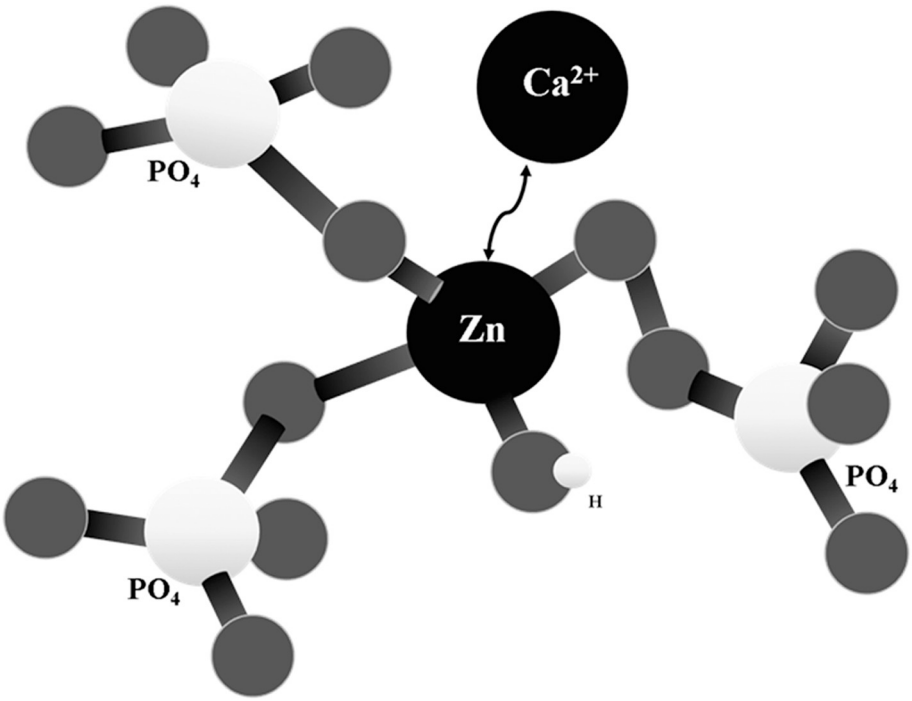

Fig. 1. Chemical structure of zinc incorporated hydroxyapatite.

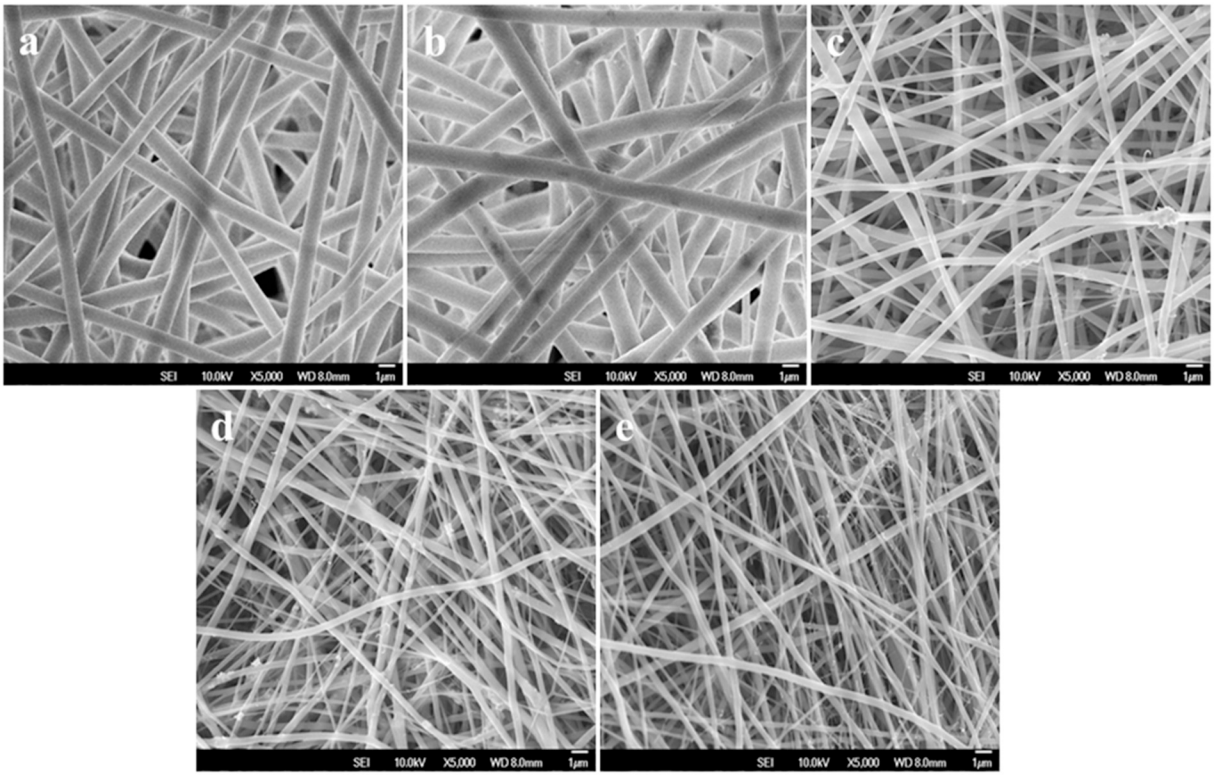

Fig. 2. SEM images for biocomposite nanofibrous scaffolds. (a) PLACL, (b) PLACL/ZnO, (c) PLACL/SF/ZnO, (d) PLACL/SF/ZnO/HAp, (e) PLACL/SF/ZnO(HAp).

analysis software (ImageJ, National Institutes of Health, USA). An average of $n = 6$ images was taken from each sample with $n = 60$ nanofibers were chosen from each image for determining the diameter of nanofibers in each sample with mean and standard deviation. Table top tensile tester (Instron 3345, USA) is used to determine the mechanical properties of electrospun biocomposite nanofibrous scaffolds with load cell of 10N capacity and intense pressure control capacity. The scaffolds were made into 10×30 mm dimension with thickness over 200–250 μm. The samples were mounted vertically into the mechanical gripping units of the Instron. Obtained results were calculated and recorded for every 50 ms over a crosshead speed of 5 mm/min at room temperature and controlled humidity. For each scaffold, $n = 6$ samples are prepared and tested. The built-in automated software (Blue Hill Materials Testing Software, Instron, USA) calculates the tensile

Table 2
Contact angles measurements for nanofibrous scaffolds.

Samples	Before plasma (°)	After plasma (°)
PLACL	139.50	26.10
PLACL/ZnO	134.40	41.70
PLACL/SF/ZnO	117.00	39.70
PLACL/SF/ZnO/HAp	133.80	44.30
PLACL/SF/ZnO(HAp)	118.30	42.90

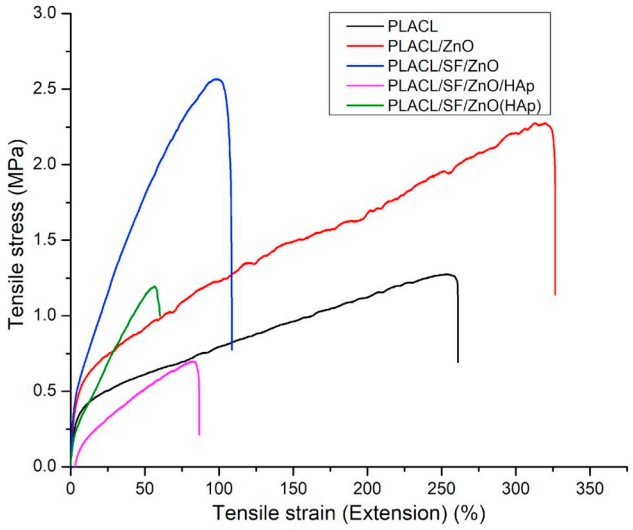

Fig. 3. Tensile properties of PLACL, PLACL/ZnO, PLACL/SF/ZnO, PLACL/SF/ZnO/HAp, PLACL/SF/ZnO(HAp) nanofibrous scaffolds.

properties such as resistance to deformation at the breaking point with the given stress and strain and load bearing capacity. Chemical and functional bonding of the samples were studied using Fourier transform infrared spectroscopy (FTIR-Avatar 380, Thermo Nicolet, Waltham, MA,USA) over the range of 400–4000 cm^{-1}. Wettability of the nanofibrous scaffolds was analysed using the video contact angle (VCA) Optima surface analysis system (AST Product, Billerica, MA). The hydrophobic samples were treated with radiofrequency glow discharge chamber (PDC-001, Harrick scientific Corporation, USA). Plasma 30 W RF was made contact for 15–30 s to convert the hydrophobic surface into hydrophilic nanofibrous scaffolds.

2.4. Culture of hFOB

Osteoblasts (hFOB) used to study the biocompatibility of electrospun nanofibrous scaffolds. The cells were cultured in DMEM/F12 medium (1:1) containing 10% FBS and 1% antibiotic and antimycotic solutions in a 75 cm^2 cell culture flask. The cells were incubated at 37 °C with intense humidity containing 5% CO_2 and sporadic change of fresh culture medium for every 2–3 days. The nanofibers were sterilized by treating ultraviolet light (UV) for 3 h. The sterilized fibers placed in 24 well plate with stainless-steel rings, in order to avoid lifting of fibers upwards followed by washing by PBS to remove the residual solvents consequently; the fibers were then kept overnight in DMEM/F12 medium before seeding cells. The confluent osteoblast cultures were trypsinized by adding 1 ml of 0.25% trypsin containing 0.1% EDTA. Trypsinized cells were centrifuged, counted by Trypan blue assay using haemocytometer. The counted cells were then seeded on TCP (control), PLACL, PLACL/ZnO, PLACL/SF/ZnO, PLACL/SF/ZnO/HAp and PLACL/SF/ZnO(HAp) nanofibrous scaffolds at the density of 1×10^4 cells per well and kept in incubator to facilitate the uninterrupted growth of cells.

2.5. hFOB proliferation

hFOB proliferation on electrospun nanofibrous scaffolds were monitored on 5, 10 and 15 days after seeding the cells. Cell proliferation was quantified using MTS assay (3-(4,5-dimethylthiazol-2-yl)-5-(3-caboxymethoxphenyl)-2-(4-sulfophenyl)-2H-tetrazolium) by Cell Titer 96® AQ_{ueous} One Solution (Promega, Madison, WI, USA). The reduction of yellow tetrazolium salts by dehydrogenase enzymes secreted by metabolically active cells break down to form purple formazan crystals. The process of MTS assay is carried out by washing with PBS to remove dead cells and incubated with 20% MTS reagent in a serum free medium for 3 h at 37 °C. The amount of formazan crystal formed varies proportionally with the number of cells. Then the samples were analysed at the absorbance range of 492 nm using FLUO star OPTIMA Spectrometric plate reader (BMG Lab Technologies).

2.6. Alkaline phosphatase activity

Alkaline phosphatase yellow liquid substrate system (Sigma Life Science, USA) was used to analyse the bone-forming ability of hFOB seeded on the biocomposite nanofibrous scaffolds. The cells were cultured for 5, 10 and 15 days and periodically subjected to ALP activity on the stipulated time periods. After washed twice with phosphate buffer saline, ALP substrate solution was added to each well and incubated for an hour, then the reaction was stopped using 2 N NaOH. Then the yellow colour developed solution from each well was transferred to 96 well plates and observed using spectrophotometric Microplate reader at an absorbance of 405 nm.

2.7. Staining of Alizarin Red-S

Mineralization of hFOB was quantified and monitored by Alizarin Red-S (ARS) staining. ARS binds to calcium salts selectively to consider the most widely used calcium mineral histochemistry (calcium chelating product). The cells scaffolds were washed twice with PBS and fixed with 70% ice-cold ethanol for an hour. After fixing with ethanol, the scaffolds were washed thrice with deionized water and stained with 40 mM ARS for 30–60 min at room temperature. Then washed with DI water to remove excess stains then captured the images under an optical microscope using image analysis software (Leica FW4000, version v 1.0.2). After a constant wash with deionized water, the scaffolds were desorbed using 10% cetylpyridinium chloride and incubate for 1 h. The dye was collected and absorbance is measured at 540–570 nm using spectrophotometer (Thermo Spectronic, Waltham, USA).

2.8. Mineralization of osteoblasts

Nanofibrous scaffolds after 9 days of the culture period, the osteoblasts cultured nanofibrous scaffolds were gently washed with PBS to remove dead cells and then fixed in 3% glutaraldehyde for 3 h at room temperature. Thereafter, the scaffolds were rinsed with distilled water

Table 3
Tensile properties of the nanofibrous scaffolds.

Sample/properties	PLACL	PLACL/ZnO	PLACL/SF/ZnO	PLACL/SF/ZnO/HAp	PLACL/SF/ZnO(HAp)
Ultimate Stress (MPa)	1.27 ± 0.15	2.25 ± 0.10	2.56 ± 0.15	0.84 ± 0.25	1.10 ± 0.20
Ultimate Strain (%)	254.00	322.4	98.2	84.3	56.4

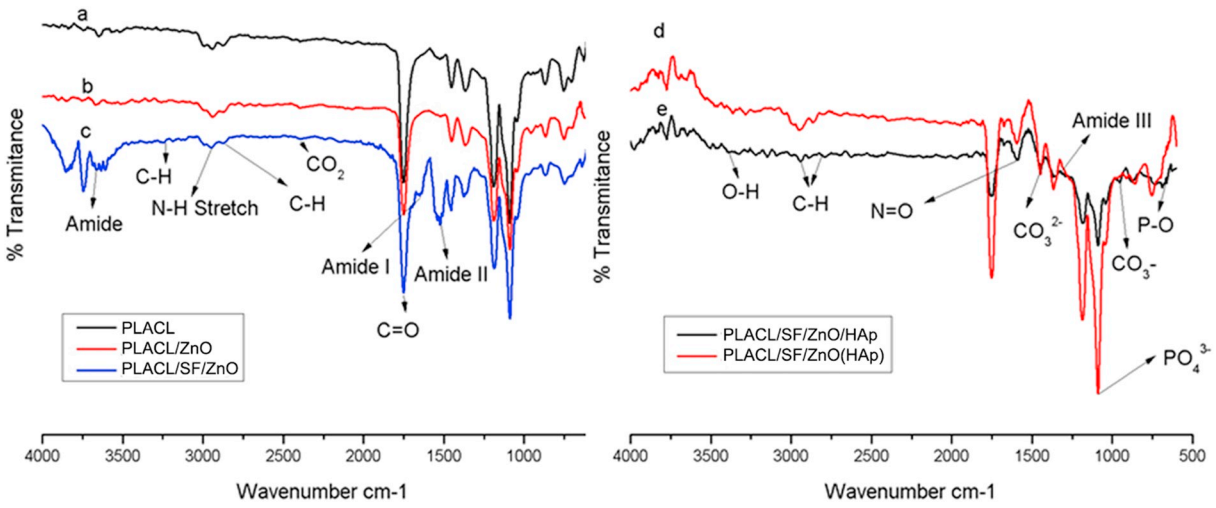

Fig. 4. FTIR spectra of biocomposite nanofibrous scaffolds. (a) PLACL, (b) PLACL/ZnO, (c) PLACL/SF/ZnO, (d) PLACL/SF/ZnO/HAp, (e) PLACL/SF/ZnO(HAp).

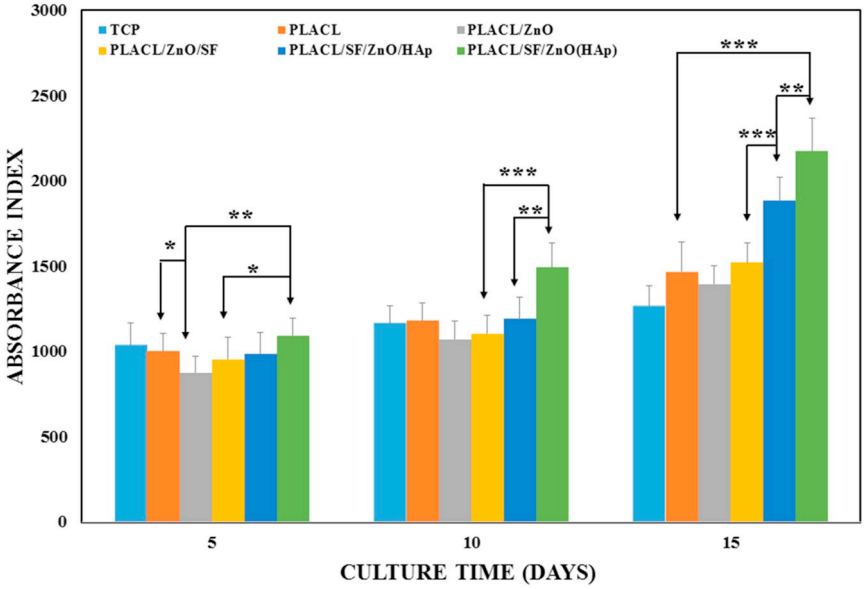

Fig. 5. Proliferation of hFOB cultured on TCP, PLACL, PLACL/ZnO, PLACL/SF/ZnO, PLACL/SF/ZnO/HAp, PLACL/SF/ZnO(HAp) biocomposite nanofibrous scaffolds. Data's are presented as mean ± standard deviation with $n = 6$ (*$P \leq 0.05$, **$P \leq 0.01$, ***$P \leq 0.001$).

and increasing the concentration of alcohol (50%, 70%, 90%, and 100%) twice with a time interval. Subsequently, the samples were added HMDS and allowed to air dry overnight in a fume hood. Then the samples were subjected to gold sputtering and observed under FESEM for the mineralization of osteoblasts.

2.9. Cell tracking using 5-chloromethylfluorescein diacetate

Multigenerational tracking of live cells monitored using the CMFDA fluorescent dye (5-chloromethylfluorescein diacetate). The cells-scaffolds were treated with CMFDA dye on day 15 and observed the morphology of live cells. The cells were incubated with dye after removal of medium and washed with PBS. Before adding 20 µl of CMFDA (25 µM) and 180 µl of DMEM is added to each wells and incubated for 2 h at 37 °C in 5% CO_2 atmosphere. After incubation, CMFDA dye was discarded and washed with PBS then by adding 1 ml of medium supplemented with 10% FBS and incubated overnight. The cells were washed twice with PBS after overnight incubation subsequently serum free medium was added and observed under inverted Leica DM IRB laser scanning microscope (Leica DC 300F) at 488 nm.

2.10. Statistical analysis

Experiments were conducted 6 times and all the data presented were expressed as mean ± standard deviation (SD). Statistical analysis was plotted using Student's *t*-test; $P \leq 0.001$ was considered to be highly significant.

3. Results and discussion

3.1. Interaction of zinc and hydroxyapatite

Interactions of zinc and hydroxyapatite in order to establish the influence of Zn on the properties of the obtained materials [35]. Zinc being the best promoter of bone growth [36], inhibits bone resorption [37], offers antimicrobial residents to implants [38] and unmatched potential form imparting multifunctional abilities in bone therapies. The incorporation of zinc helps in maintaining the pH in simulating body fluid (SBF) within physiological limits. Antibacterial activity of Zn doped hydroxyapatite was investigated by Stanić et al. providing the activities of biocomposite ZnO-HAp [39]. Zhou et al. reported the

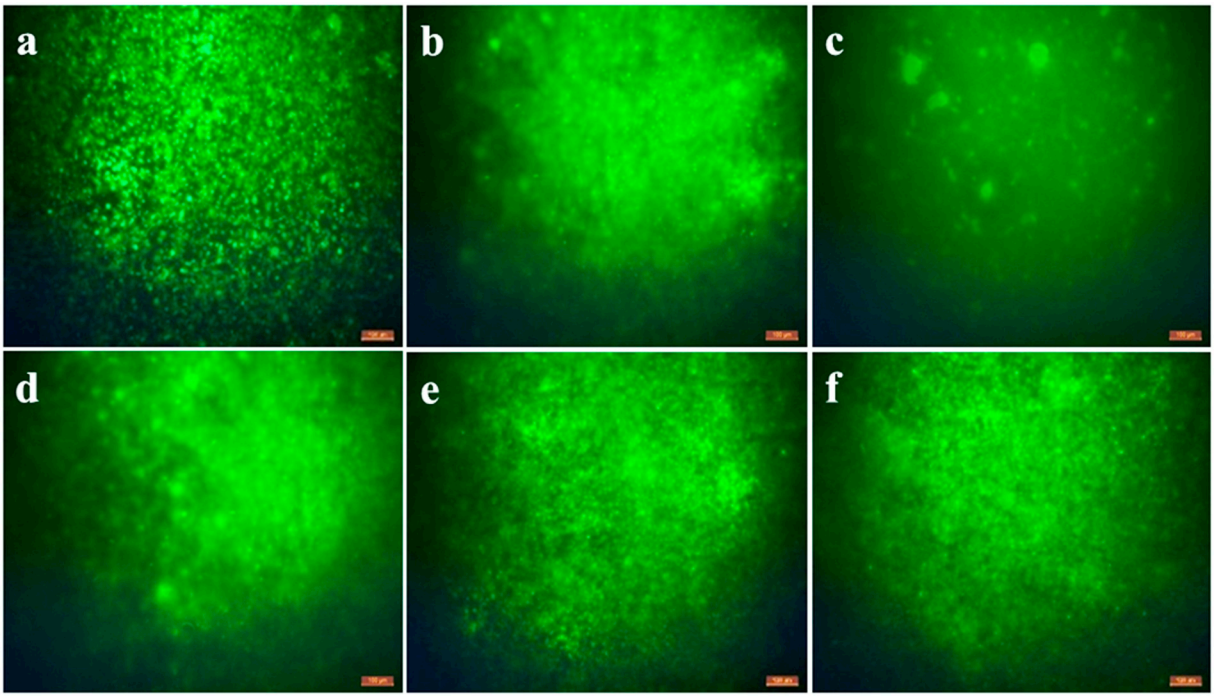

Fig. 6. CMFDA live cell imaging on biocomposite nanofibrous scaffolds on day 15. (a) TCP, (b) PLACL, (c) PLACL/ZnO, (d) PLACL/SF/ZnO, (e) PLACL/SF/ZnO/HAp, (f) PLACL/SF/ZnO(HAp).

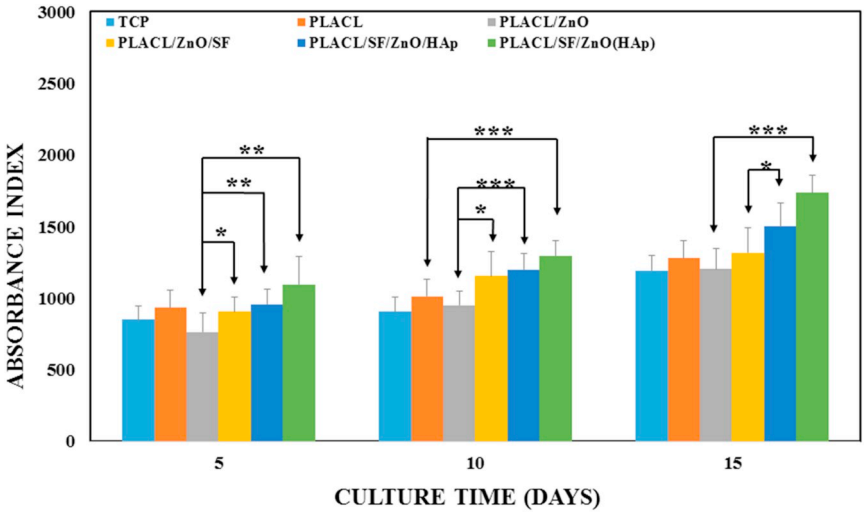

Fig. 7. Alkaline phosphatase (ALP) activity in hFOB cultured on TCP, PLACL, PLACL/ZnO, PLACL/SF/ZnO, PLACL/SF/ZnO/HAp, PLACL/SF/ZnO(HAp) biocomposite nanofibrous scaffolds. Data's are presented as mean ± standard deviation with $n = 7$(*$P \leq 0.05$, **$P \leq 0.01$, ***$P \leq 0.001$).

synthesis through a precipitation process, characterization and antimicrobial activities of a nanohydroxyapatite/zinc oxide complex [40]. Other studies related to zinc incorporation into hydroxyapatite revealed that zinc replaces calcium in hydroxyapatite structures [41] and as depicted in Fig. 1. Zinc (Zn^{2+}) is proven to stimulate the bone mineral secretion in osteoblast cells [42]. Incorporation process of zinc and hydroxyapatite can be simply explained as; isovalent Ca^{2+} in HAp is replaced by Zn^{2+} ions shown below:

$$Ca^{2+}_{(10-x)} + Zn^{2+}_{x} + 6PO^{3-}_{4} + 2OH^{-} \rightarrow Ca_{(10-x)}Zn_{x}(PO_4)_6(OH)_2;\ (0 \leq x \leq 10)$$

$$Ca^{2+}{}_{x}(HAp) + Zn^{2+}(aqus) \rightarrow Zn_{x}(HAp)(Ca^{2+})$$

Chemical scheme: Local coordination of zinc in hydroxyapatite and releasing the calcium ions.

Previous experiments showed Zn^{2+} doped HAp precipitated from aqueous solution often showed number of Ca^{2+} vacancy. Later it was described that Zn^{2+} incorporation into HAp does not occur by simple replacement of ions but Ca^{2+} vacancy defect forms a plausible atomic sites for substituting Zn^{2+} in HAp [43]. Most of the cases Zn^{2+} ions prefers the Ca^{2+} site next to the hydroxyl column rather than Ca1 site upon incorporation [41,43]. It should be noted that substitutional Zn^{2+} and the defect complex shows attractive interaction and energetically favour the associated structure as shown in Fig. 1. Looking more closely at the Fig. 1, shows that four oxygen atoms bonded to Zn, one from nearest hydroxyl group and three from adjacent phosphate (PO_4) groups [44,45].

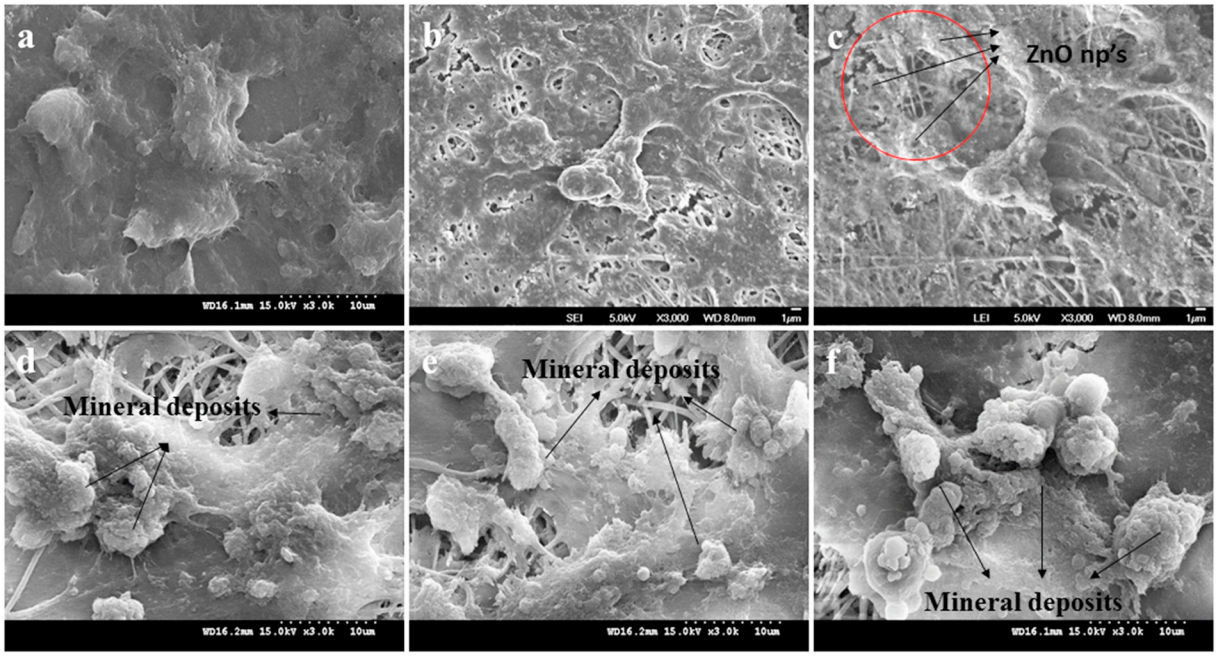

Fig. 8. SEM images of mineralization on the biocomposite nanofibrous scaffolds on day 15. (a) TCP, (b) PLACL, (c) PLACL/ZnO, (d) PLACL/SF/ZnO, (e) PLACL/SF/ZnO/HAp, (f) PLACL/SF/ZnO(HAp).

3.2. Morphology of nanofibrous scaffolds

The nanofiber surface topography plays a crucial role in regulating initial cell behaviour, such as cell adhesion, which can also influence cell viability, proliferation and differentiation in later stages of cells. SEM images reveal the fiber diameter reduced after addition of silk fibroin and HAp. Compared to PLACL and PLACL/ZnO fiber diameter was larger slightly 715.4 ± 190 nm over 627.3 ± 103 nm. The ZnO doped HAp fibers taking lead with a very small fiber diameter of 139.4 ± 27 nm with very slight standard deviation variations of PLACL/SF/ZnO and PLACL/SF/ZnO(HAp) fibers with 192 ± 69 nm and 139.4 ± 27 nm respectively (Fig. 2).

3.3. Wettability of the nanofibrous scaffolds

Hybrid scaffolds with natural polymers imparts functional groups like amide, ester and hydroxyl groups making the scaffolds hydrophilic to favour cell adhesion and proliferation [46]. Silk fibroin providing amide groups which represents hydrophilic were as the other constituents in the hydride scaffold like PLACL, ZnO particles lack this ability which are in maximum percentage thus considering hydrophobic. The contact angle studies (Table 2) showed the fibrous scaffolds was wetting the surface between 25 and 47° which comes under hydrophilic nature. All the scaffolds were hydrophobic later converted to hydrophilic by the influence of plasma on their surface of the fibers. During plasma treatment, the formation of polar bonds on the surface of the nanofibrous scaffolds modifies the surface energy suitable for wetting the surface thus results the samples to use for tissue engineering applications.

3.4. Tensile properties of the nanofibers

Tissue engineering systems are highly dependent on the chemical stability and mechanical properties of the scaffolds, which shows a huge impact on cell proliferation and growth of the tissues. However HAp has a major role in boosting the mineral secretion and low tensile strength, brittleness hampers its application to the hard tissue implants [47,48]. Fig. 3/Table 3 shows the stress-strain curves for PLACL, PLACL/ZnO, PLACL/SF/ZnO, PLACL/SF/ZnO/HAp and PLACL/SF/ZnO(HAp) biocomposite nanofibrous scaffolds under normal room temperature. The bonding of ZnO nanoparticles with PLACL fibers shows the maximum elastic strain percentage 322.4% among other scaffolds and showing second maximum ultimate stress at 2.25 ± 0.10 MPa along with the lead PLACL/SF/ZnO scaffolds with 2.56 ± 0.15 MPa showing less elastic strain percentage of 98.2%. The incorporation of silk fibroin increases the yield strength by breaking the bondage between ZnO particles with PLACL polymer showing a reduction in strain. The interphase between the crystals, semicrystalline region and shear alignment of the molecular chain are the fundamental foundations for silk's unique mechanical properties due to the combination of β-sheet crystals [13]. The highly organized β-sheet regions of protein provide the high tensile activity, tensile integrity, semicrystalline regions are the basis for the proteins elastic nature [49]. Comparing PLACL/SF/ZnO/HAp and PLACL/SF/ZnO(HAp) scaffolds both lack in tensile strength with respect to the other fibers and showing elastic breaking percentage of 84.3% and 56.4% respectively. Within the ZnO and HAp fibers, the one which has doped content shows the maximum yield strength 1.1 ± 0.20 MPa by losing the strain with the other nanofibrous scaffolds.

3.5. Functional groups of fibrous scaffolds

The IR spectra of electrospun nanofibers PLACL, PLACL/ZnO, PLACL/SF/ZnO, PLACL/SF/ZnO/HAp and PLACL/SF/ZnO(HAp) were studied using Fourier transform infrared spectroscopy (Fig. 4). The characteristics peaks were noted at 2951.08 and 1749.43 cm^{-1} representing nitrogen group (amine) (N—H Stretch) and C=O ketone, C—H stretching at 3243.33 cm^{-1} for amide. The spectra of prepared ZnO nanoparticles occurred in the range of 4000–400 cm^{-1} at room temperature. The peak at 3463 cm^{-1} represents the presence of hydrogen bond O—H stretch and peaks at 2382.37 cm^{-1} represents the CO_2. The peaks 2862.36, 2922.59 and 2855.05 cm^{-1} represents the C—H stretch on the nanofibrous scaffolds. Amide I, II and III are shown at 1646.44, 1520.44 and 1269.02 cm^{-1}. Stretching vibration of PO_4^{3-} from mineral HAp was obtained at 1087.85 and 1020.10 cm^{-1} for P—O stretch at 589.14 cm^{-1} for P—O stretch coupled with P—O bend with

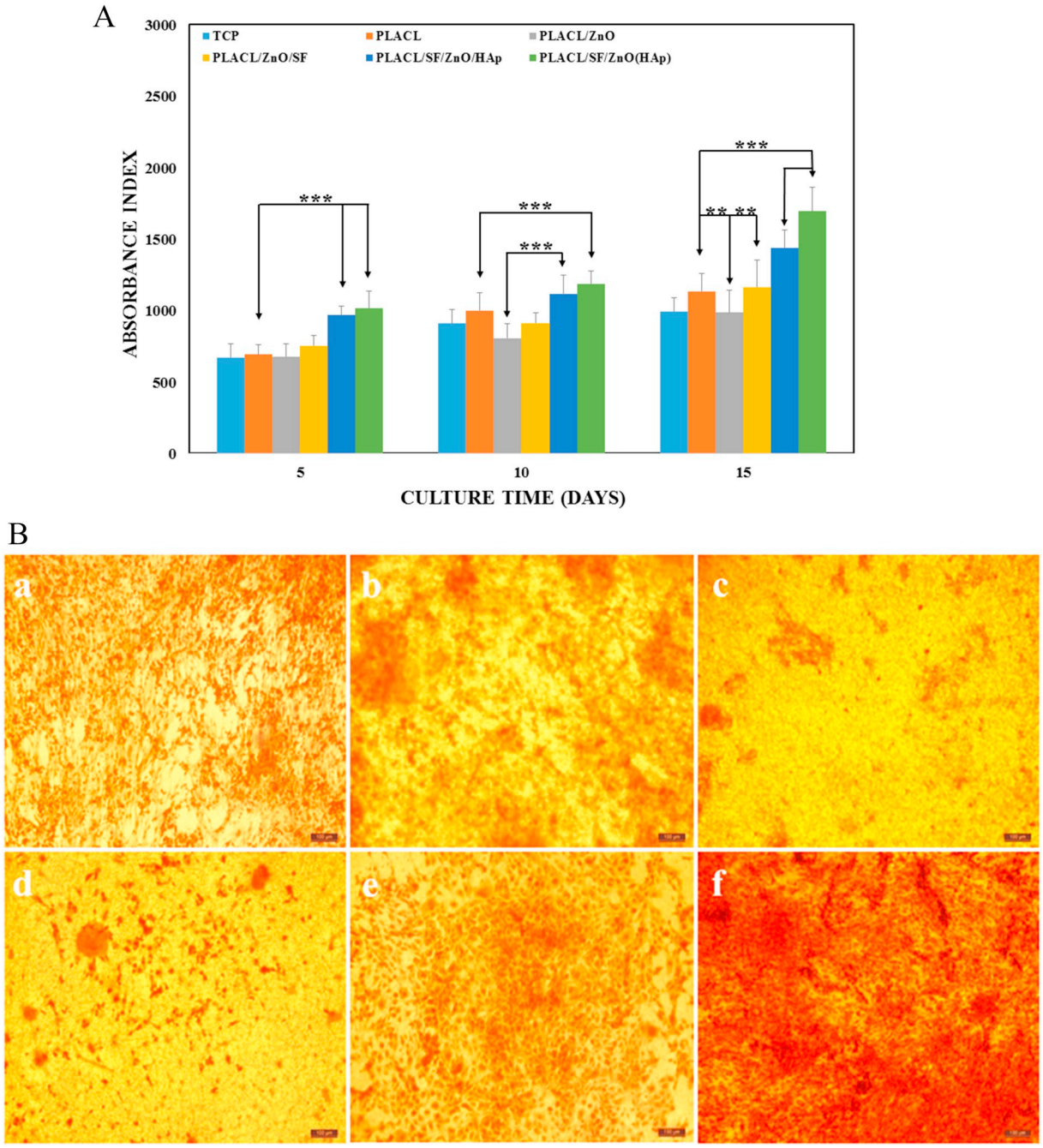

Fig. 9. A. Quantification of mineral deposits in hFOB by ARS staining on TCP, PLACL, PLACL/ZnO, PLACL/SF/ZnO, PLACL/SF/ZnO/HAp, PLACL/SF/ZnO(HAp) biocomposite nanofibrous scaffolds. Data's are presented as mean ± standard deviation with $n = 10$ ($^{**}P \leq 0.01$, $^{***}P \leq 0.001$)
B. Alizarin Red staining for the mineralization of osteoblasts on day 15. (a) TCP, (b) PLACL, (c) PLACL/ZnO, (d) PLACL/SF/ZnO, (e) PLACL/SF/ZnO/HAp, (f) PLACL/SF/ZnO(HAp) biocomposite nanofibrous scaffolds. (For interpretation of the references to colour in this figure legend, the reader is referred to the web version of this article.)

sharper peak for HAp nanofibers pertaining to 948.12 and 980.00 cm^{-1}. Ca_3^{2-} group from carbonate substituted OH and PO_4^{3-} group in HAp were obtained at about 1400–1480 cm^{-1} range (Fig. 4d,e). Phosphate group 1000–1150 cm^{-1} indicates organic-inorganic interaction between HAp crystals.

3.6. Proliferation of hFOB and live cell imaging

Biomimic ECM native environment for the scaffolds should be favourable for cell adhesion, proliferation and provides exchange of vital nutrients to grow cells to promote the secretion of bone mineral matrix. A huge number of cross-linked and rough surface nanofibrous scaffolds support the proliferation of osteoblasts and faster regeneration process of the defective bone. In addition to that suitable mechanical properties, hydrophilic nature, biomolecular signals from the nanofibers may also guide cells entering the cell substrates by their amoeboid movement [50]. The obtained results observed in Fig. 5, showing the cell growth on day 5, there was increased cell proliferation on day 15 on the progression of different fibrous scaffolds. It was found that the PLACL/ZnO nanofibrous scaffolds showed less proliferation on comparing to TCP from the beginning of the study on day 5 and later in day 10 increased to 10%. Compared to PLACL with ZnO incorporated HAp

nanofibrous scaffolds showed significantly ($P \leq 0.001$) increased on day 15, which was 48% growth comparing ZnO/HAp scaffolds on the same day with only 28% proliferation. The overall study, the highest significant ($P \leq 0.001$) level of increase in cell growth by 98% in ZnO incorporated HAp nanofibrous scaffolds, which proves the increased mineral secretion as shown in ARS imaging in Fig. 9. Fluorescent imaging is ventured on the cells seeded nanofibrous scaffolds under the influence of 5-chloromethylfluorescein diacetate dye (CMFDA) shown in Fig. 6. hFOB proliferated higher levels in ZnO and HAp doped nanofibrous scaffolds (Fig. 6e,f) compared to all other nanofibrous scaffolds. Whereas on PLACL/ZnO nanofibers (Fig. 6c) showing lesser cells and abnormal cell morphology compared to PLACL/SF/ZnO/HAp scaffolds.

3.7. ALP activity and mineralization of hFOB

ALP activity analysed for cells-scaffolds during the period of day 5, 10 and 15 showed in Fig. 7. ZnO(HAp) scaffolds observed significantly increased ALP activity upto 44% on day 15 compared PLACL/ZnO fibers on day 5. PLACL scaffolds with ZnO(HAp) composite on day 10 and 15 shows significantly ($P \leq 0.01$) increased activity by 28% and 35% respectively (Fig. 7). ALP activity directly related to the mineralization of ECM for forming bone minerals and nodules. The cell density is observed confluent on day 15 of all nanofibrous scaffolds and mineralization of the samples related to ZnO(HAp) doped samples showing increased bone mineral formation (Fig. 8). Mineralization phase begins with the secretion of mineral matrix upon undergoing osteogenic differentiation. Feng et al. proved β-TCP scaffolds doped with ZnO possessed good mechanical properties and excellent biocompatibility for bone tissue engineering [51]. HAp acts as a chelating agent in PLACL/SF/ZnO/HAp and PLACL/SF/ZnO(HAp) scaffolds for the mineralization of osteoblasts. Fig. 8f showing huge bone minerals formation for proving that the PLACL/SF/ZnO(HAp) have good potentiality for bone tissue regeneration. The higher concentration of ZnO present in the fibers are not shown mineralization on day 15 compared to ZnO(HAp) doped biocomposite nanofibrous scaffolds (Figs. 8, 9). ZnO doped HAp biocomposite nanofibrous scaffolds showed 71% growth progression for the secretion of minerals in Fig. 9a compared to PLACL/ZnO. Mineralization was clearly observed on day 15 in PLACL/SF/ZnO(HAp) scaffolds compared to PLACL and PLACL/ZnO fibers as indicated in Fig. 9b related to the cell proliferation upto 49% as described in Fig. 5. The presence of ZnO/SF/(HAp) in PLACL biocomposites nanofibrous scaffolds proved increased cell proliferation, ALP activity and mineralization for the obtained results, these biocomposite material systems have proved the potentials for bone regenerative therapy.

4. Conclusion

Harnessed a nanofiber that can mimic extracellular matrix by providing a suitable microenvironment that can help in greater mineralization of osteoblasts. The experimental results proved two factors that ZnO/SF promotes the cell proliferation and ZnO incorporated/doped HAp scaffolds trigger the cells for a higher level of bone minerals secretion for the formation of bone. As stated above, these fabricated scaffolds have increased mineralization but lack mechanical strength due to the hydroxyapatite crystallinity. ZnO/SF incorporated/doped hydroxyapatite in tissue engineering will provide a huge platform to increase the studies on these metal oxide doped hydroxyapatite biocomposites in further days for bone regenerative therapy.

Acknowledgement

This study was supported by the Department of Mechanical Engineering, National University of Singapore, Singapore and Faculty of Industrial Sciences & Technology, Universiti Malaysia Pahang, Malaysia.

References

[1] V.D. Rani, K. Manzoor, D. Menon, N. Selvamurugan, S.V. Nair, The design of novel nanostructures on titanium by solution chemistry for an improved osteoblast response, Nanotechnology 20 (19) (2009) 195101.
[2] F. Kaplan, W. Hayes, T. Keaven, Orthopaedic Basic Science, American Academy of Orthopaedic Surgeons, Columbus OH, 1994.
[3] L. Zhao, E.F. Burguera, H.H. Xu, N. Amin, H. Ryou, D.D. Arola, Fatigue and human umbilical cord stem cell seeding characteristics of calcium phosphate–chitosan–biodegradable fiber scaffolds, Biomaterials 31 (5) (2010) 840–847.
[4] Z. Huang, J. Tian, B. Yu, Y. Xu, Q. Feng, A bone-like nano-hydroxyapatite/collagen loaded injectable scaffold, Biomed. Mater. 4 (5) (2009) 055005.
[5] K. Zhao, Y. Deng, J.C. Chen, G.-Q. Chen, Polyhydroxyalkanoate (PHA) scaffolds with good mechanical properties and biocompatibility, Biomaterials 24 (6) (2003) 1041–1045.
[6] S. Holland, M. Yasin, B. Tighe, Polymers for biodegradable medical devices: VII. Hydroxybutyrate-hydroxyvalerate copolymers: degradation of copolymers and their blends with polysaccharides under in vitro physiological conditions, Biomaterials 11 (3) (1990) 206–215.
[7] J.W. Rhim, A.K. Mohanty, S.P. Singh, P.K. Ng, Effect of the processing methods on the performance of polylactide films: thermocompression versus solvent casting, J. Appl. Polym. Sci. 101 (6) (2006) 3736–3742.
[8] C.M. Agrawal, K.A. Athanasiou, Technique to control pH in vicinity of biodegrading PLA-PGA implants, J. Biomed. Mater. Res. 38 (2) (1997) 105–114.
[9] J.C. Middleton, A.J. Tipton, Synthetic biodegradable polymers as orthopedic devices, Biomaterials 21 (23) (2000) 2335–2346.
[10] H. Kweon, M.K. Yoo, I.K. Park, T.H. Kim, H.C. Lee, H.-S. Lee, J.-S. Oh, T. Akaike, C.-S. Cho, A novel degradable polycaprolactone networks for tissue engineering, Biomaterials 24 (5) (2003) 801–808.
[11] A. Akkouch, Z. Zhang, M. Rouabhia, A novel collagen/hydroxyapatite/poly (lactide-co-ε-caprolactone) biodegradable and bioactive 3D porous scaffold for bone regeneration, J. Biomed. Mater. Res. A 96 (4) (2011) 693–704.
[12] H. Yoshimoto, Y. Shin, H. Terai, J. Vacanti, A biodegradable nanofiber scaffold by electrospinning and its potential for bone tissue engineering, Biomaterials 24 (12) (2003) 2077–2082.
[13] S. Nagarkar, A. Patil, A. Lele, S. Bhat, J. Bellare, R. Mashelkar, Some mechanistic insights into the gelation of regenerated silk fibroin sol, Ind. Eng. Chem. Res. 48 (17) (2009) 8014–8023.
[14] O. Yamamoto, T. Ohira, K. Alvarez, M. Fukuda, Antibacterial characteristics of CaCO 3–MgO composites, Mater. Sci. Eng. B 173 (1) (2010) 208–212.
[15] S.V. Sudakaran, J.R. Venugopal, G.P. Vijayakumar, S. Abisegapriyan, A.N. Grace, S. Ramakrishna, Sequel of MgO nanoparticles in PLACL nanofibers for anti-cancer therapy in synergy with curcumin/β-cyclodextrin, Mater. Sci. Eng. C 71 (2017) 620–628.
[16] P. Dallas, V.K. Sharma, R. Zboril, Silver polymeric nanocomposites as advanced antimicrobial agents: classification, synthetic paths, applications, and perspectives, Adv. Colloid Interf. Sci. 166 (1) (2011) 119–135.
[17] R. Prucek, J. Tucek, M. Kilianova, A. Panacek, L. Kvitek, J. Filip, M. Kolar, K. Tomankova, R. Zboril, The targeted antibacterial and antifungal properties of magnetic nanocomposite of iron oxide and silver nanoparticles, Biomaterials 32 (21) (2011) 4704–4713.
[18] N.A. Trujillo, R.A. Oldinski, H. Ma, J.D. Bryers, J.D. Williams, K.C. Popat, Antibacterial effects of silver-doped hydroxyapatite thin films sputter deposited on titanium, Mater. Sci. Eng. C 32 (8) (2012) 2135–2144.
[19] Y.-H. Chan, C.-F. Huang, K.-L. Ou, P.-W. Peng, Mechanical properties and antibacterial activity of copper doped diamond-like carbon films, Surf. Coat. Technol. 206 (6) (2011) 1037–1040.
[20] C. Dong, D. Song, J. Cairney, O.L. Maddan, G. He, Y. Deng, Antibacterial study of Mg (OH) 2 nanoplatelets, Mater. Res. Bull. 46 (4) (2011) 576–582.
[21] B.A. Çakır, L. Budama, Ö. Topel, N. Hoda, Synthesis of ZnO nanoparticles using PS-b-PAA reverse micelle cores for UV protective, self-cleaning and antibacterial textile applications, Colloids Surf. A Physicochem. Eng. Asp. 414 (2012) 132–139.
[22] L. Trandafilović, D. Božanić, S. Dimitrijević-Branković, A. Luyt, V. Djoković, Fabrication and antibacterial properties of ZnO–alginate nanocomposites, Carbohydr. Polym. 88 (1) (2012) 263–269.
[23] M.J. Osmond, M.J. Mccall, Zinc oxide nanoparticles in modern sunscreens: an analysis of potential exposure and hazard, Nanotoxicology 4 (1) (2010) 15–41.
[24] J.W. Rasmussen, E. Martinez, P. Louka, D.G. Wingett, Zinc oxide nanoparticles for selective destruction of tumor cells and potential for drug delivery applications, Expert Opin. Drug Deliv. 7 (9) (2010) 1063–1077.
[25] W. Song, C. Wu, H. Yin, X. Liu, P. Sa, J. Hu, Preparation of PbS nanoparticles by phase-transfer method and application to Pb^{2+}-selective electrode based on PVC membrane, Anal. Lett. 41 (15) (2008) 2844–2859.
[26] M. Bohner, Physical and chemical aspects of calcium phosphates used in spinal surgery, Eur. Spine J. 10 (2) (2001) S114–S121.
[27] M.-P. Ginebra, T. Traykova, J. Planell, Calcium phosphate cements as bone drug delivery systems: a review, J. Control. Release 113 (2) (2006) 102–110.
[28] I.R.d. Lima, A.M. Costa, I.N. Bastos, J.M. Granjeiro, G.d.A. Soares, Development and characterization of 5% mol Zn bioceramic in granular form, Mater. Res. 9 (4) (2006) 399–403.
[29] X. Wei, M. Akinc, Si, Zn-modified tricalcium phosphates: a phase composition and crystal structure study, Key Eng. Mater., Trans. Tech. Publ. (2005) 83–88.
[30] P. Bhattacharjee, H. Begam, A. Chanda, S.K. Nandi, Animal trial on zinc doped

hydroxyapatite: a case study, J. Asian Ceramic Soc. 2 (1) (2014) 44–51.
[31] A. Bigi, E. Foresti, M. Gandolfi, M. Gazzano, N. Roveri, Isomorphous substitutions in β-tricalcium phosphate: the different effects of zinc and strontium, J. Inorg. Biochem. 66 (4) (1997) 259–265.
[32] R. Legeros, C. Bleiwas, M. Retino, R. Rohanizadeh, J. Legeros, Zinc effect on the in vitro formation of calcium phosphates: relevance to clinical inhibition of calculus formation, Am. J. Dent. 12 (2) (1999) 65–71.
[33] X. Xiao, R. Liu, C. Chen, L. Huang, Structural characterization of zinc-substituted hydroxyapatite prepared by hydrothermal method, J. Mater. Sci. Mater. Med. 19 (2) (2008) 797–803.
[34] A. Ito, M. Otsuka, H. Kawamura, M. Ikeuchi, H. Ohgushi, Y. Sogo, N. Ichinose, Zinc-containing tricalcium phosphate and related materials for promoting bone formation, Curr. Appl. Phys. 5 (5) (2005) 402–406.
[35] A. Oki, B. Parveen, S. Hossain, S. Adeniji, H. Donahue, Preparation and in vitro bioactivity of zinc containing sol-gel–derived bioglass materials, J. Biomed. Mater. Res. A 69 (2) (2004) 216–221.
[36] M. Yamaguchi, H. Oishi, Y. Suketa, Stimulatory effect of zinc on bone formation in tissue culture, Biochem. Pharmacol. 36 (22) (1987) 4007–4012.
[37] B.S. Moonga, D.W. Dempster, Zinc is a potent inhibitor of osteoclastic bone resorption in vitro, J. Bone Miner. Res. 10 (3) (1995) 453–457.
[38] J.F. Hernández-Sierra, F. Ruiz, D.C.C. Pena, F. Martínez-Gutiérrez, A.E. Martínez, A.d.J.P. Guillén, H. Tapia-Pérez, G.M. Castañón, The antimicrobial sensitivity of *Streptococcus mutans* to nanoparticles of silver, zinc oxide, and gold, Nanomedicine 4 (3) (2008) 237–240.
[39] V. Stanić, S. Dimitrijević, J. Antić-Stanković, M. Mitrić, B. Jokić, I.B. Plećaš, S. Raičević, Synthesis, characterization and antimicrobial activity of copper and zinc-doped hydroxyapatite nanopowders, Appl. Surf. Sci. 256 (20) (2010) 6083–6089.
[40] G. Zhou, Y. Li, W. Xiao, L. Zhang, Y. Zuo, J. Xue, J.A. Jansen, Synthesis, characterization, and antibacterial activities of a novel nanohydroxyapatite/zinc oxide complex, J. Biomed. Mater. Res. A 85 (4) (2008) 929–937.
[41] Y. Tang, H.F. Chappell, M.T. Dove, R.J. Reeder, Y.J. Lee, Zinc incorporation into hydroxylapatite, Biomaterials 30 (15) (2009) 2864–2872.
[42] H. Kawamura, A. Ito, S. Miyakawa, P. Layrolle, K. Ojima, N. Ichinose, T. Tateishi, Stimulatory effect of zinc-releasing calcium phosphate implant on bone formation in rabbit femora, J. Biomed. Mater. Res. 50 (2) (2000) 184–190.
[43] K. Matsunaga, First-principles study of substitutional magnesium and zinc in hydroxyapatite and octacalcium phosphate, J. Chem. Phys. 128 (24) (2008) 245101.
[44] J. Terra, M. Jiang, D. Ellis, Characterization of electronic structure and bonding in hydroxyapatite: Zn substitution for Ca, Philos. Mag. A 82 (11) (2002) 2357–2377.
[45] J. Venugopal, M.P. Prabhakaran, S. Low, A.T. Choon, Y. Zhang, G. Deepika, S. Ramakrishna, Nanotechnology for nanomedicine and delivery of drugs, Curr. Pharm. Des. 14 (22) (2008) 2184–2200.
[46] A.I. Teixeira, P.F. Nealey, C.J. Murphy, Responses of human keratocytes to micro- and nanostructured substrates, J. Biomed. Mater. Res. A 71A (3) (2004) 369–376.
[47] H.-W. Kim, S.-Y. Lee, C.-J. Bae, Y.-J. Noh, H.-E. Kim, H.-M. Kim, J.S. Ko, Porous ZrO_2 bone scaffold coated with hydroxyapatite with fluorapatite intermediate layer, Biomaterials 24 (19) (2003) 3277–3284.
[48] R.E. Holmes, R. Bucholz, V. Mooney, Porous hydroxyapatite as a bone-graft substitute in metaphyseal defects. A histometric study, J. Bone Joint Surg. 68 (6) (1986) 904–911.
[49] Q. Zhang, S. Yan, M. Li, Silk fibroin based porous materials, Materials 2 (4) (2009) 2276–2295.
[50] J.R. Venugopal, S. Low, A.T. Choon, A.B. Kumar, S. Ramakrishna, Nanobioengineered electrospun composite nanofibers and osteoblasts for bone regeneration, Artif. Organs 32 (5) (2008) 388–397.
[51] P. Feng, P. Wei, C. Shuai, S. Peng, Characterization of mechanical and biological properties of 3-D scaffolds reinforced with zinc oxide for bone tissue engineering, PLoS One 9 (1) (2014) e87755.